Corrections to the strong-stretching theory of polymer brushes due to the entropy of the free ends

M. W. Matsen[a)]
Polymer Science Centre, University of Reading, Whiteknights, Reading RG6 6AF, United Kingdom

(Received 5 March 2002; accepted 30 April 2002)

The entropy associated with the free ends of a polymer brush is incorporated into the standard analytical strong-stretching theory (SST). The resulting corrections are found to have a significant effect on the end-segment distribution function, the self-consistent field, the brush profile, and the polymer trajectories. This alone is enough to bring many of the SST predictions into good agreement with the more complete numerical self-consistent field theory (SCFT). Furthermore, the corrections, in most cases, obey simple scaling expressions that remain accurate down to experimentally relevant grafting densities. This encouraging result suggests that, with further corrections, an analytical SST could be developed capable of quantitatively competing with SCFT. © *2002 American Institute of Physics.* [DOI: 10.1063/1.1487819]

I. INTRODUCTION

Two distinct but intimately related theories have emerged for the study of polymer brushes and likewise block copolymers. We refer to the self-consistent field theory (SCFT) introduced by Edwards[1] in 1965, and the strong-stretching theory (SST) formulated by Semenov[2] in 1985. In reality, both theories are based on the same underlying Gaussian chain model.[3] The difference is that SCFT represents the full mean-field treatment, whereas SST is an approximation that assumes the chains are strongly stretched. The advantage of SST is that it provides simple analytical predictions, while SCFT has to be, in general, solved numerically. Unfortunately, the stringent assumptions of SST are not fully realized at experimentally relevant grafting densities. In fact, even the SCFT calculations,[4,5] performed at degrees of stretching well beyond those characteristic of experiment, have yet to reach a regime where the SST assumptions are accurate.

There is a wide assortment of polymeric systems to which these two versatile theories apply. Here, we examine one of the simplest, that involving two opposing brushes as illustrated in Fig. 1. This system is particularly fundamental because first of all it is a single component system, and second of all it provides a basis for understanding block copolymer melts.[2] Due to its inherent simplicity, it is controlled by just one parameter, $L/aN^{1/2}$, the ratio of the brush thickness to the natural end-to-end length of the grafted chains. (Note that a is the statistical segment length, and N is the number of segments per polymer chain.) Experiments are generally performed at $L/aN^{1/2} \lesssim 1$, whereas the SST assumes $L/aN^{1/2} \gg 1$. To help bridge this gap, theorists have examined the entropic correction due to the free ends of the brush,[6] the effect of fluctuations in the chain trajectory,[7] and most recently the effect of a so-called *proximal* layer at the base of each brush.[8] This paper revisits the first of these corrections in greater detail.

An interesting feature of polymeric brushes is the fact that, even though all chains are identical, their free ends extend over a wide range of distances, z_0, from the grafting surface. Nevertheless, according to the conventional SST, the distribution of chain ends, $g(z_0)$, is identically zero for $z_0 > L$. In other words, the two opposing brushes remain completely separated with none of their respective chains ever crossing the midplane at $z=L$. Witten *et al.*[9] recognized that including end-segment entropy into the SST would provide $g(z_0)$ with an exponentially decaying tail protruding beyond the midplane, thus creating a narrow interpenetration zone where the two brushes would mix. Furthermore, they argued that the width of the interpenetration zone would scale as $L^{-1/3}$. However, an exact analytical treatment of this behavior was not possible due to its complicated effect on the self-consistent field, $w(z)$, used to enforce a uniform polymer density. Matsen and Bates[6] over came this complication by solving $w(z)$ numerically, and furthermore showed that the resulting $g(z_0)$ was in good agreement with SCFT. Although their numerical calculation confirmed the $L^{-1/3}$ scaling of the tail, it also demonstrated that the interpenetration zone was by no means narrow for experimentally relevant conditions.

Here, we extend the previous calculations in Ref. 6, examining not only the end-segment distribution function, $g(z_0)$, but also the brush profile, $\phi(z)$, and the effect on the free energy per chain, f. We also improve upon the previous numerical treatment by allowing for nonmonotonic trajectories, as suggested by the more recent work of Netz and Schick.[10] Our study focuses primarily on the scaling behavior associated with the entropic corrections due to the free ends. In particular, we confirm the scaling exponents predicted earlier, evaluate the proportionality constants, and examine the range over which the scaling behavior is applicable. Furthermore, we assess the effectiveness of these SST corrections with direct comparisons to SCFT.

[a)]Electronic mail: m.w.matsen@reading.ac.uk

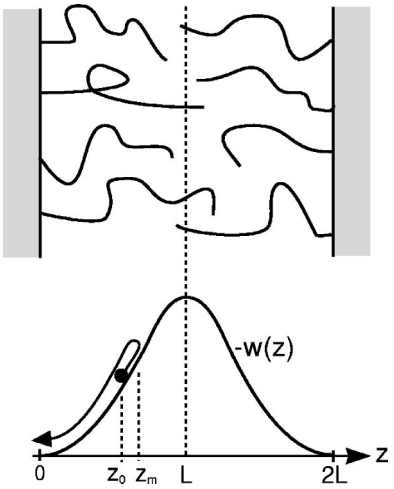

FIG. 1. Schematic diagram of two opposing brushes grafted to the substrates at $z=0$ and $z=2L$ such that they interpenetrate at the $z=L$ midplane indicated by a dashed line. The diagram below illustrates how the z-coordinate of a SST trajectory, $z_\alpha(s)$, is obtained by mapping the problem onto that of a particle sliding down a frictionless hill, with a height equal to minus the self-consistent field, $-w(z)$. In this particular example, the particle starts at $z=z_0$, moves up the hill until it reaches $z=z_m$, and then reverses direction eventually ending up at the $z=0$ substrate.

II. SELF-CONSISTENT FIELD THEORY

This section presents the self-consistent field theory (SCFT) for a pair of identical opposing polymer brushes attached to flat parallel substrates at $z=0$ and $z=2L$ (see Fig. 1). Each chain in the two brushes will have a natural end-to-end length of $aN^{1/2}$, where a is the statistical segment length and N is its total number of segments per chain. However, the chains are forced to stretch beyond their natural length in order to prevent overcrowding at the substrates. This is necessitated by the hard-core interactions between the segments, but unfortunately a rigorous theoretical treatment of these interactions is not possible. Thus, in the spirit of mean-field theory, they are mimicked by a static field, $w(z)$, which is determined self-consistently by requiring a uniform segment density.[3]

Before tackling the polymer brush problem, we first consider a short length of chain with sN segments $(0<s<1)$ occupying a trajectory given by $\mathbf{r}_\alpha(t)=(x_\alpha(t),y_\alpha(t),z_\alpha(t))$, where $0<t<s$. Furthermore, we assume that the chain ends are fixed such that $z_\alpha(0)=z_0$ and $z_\alpha(s)=z$. In this particular case, where the field depends only on z, the energy of the chain can be split into a parallel contribution,

$$\frac{\hat{E}_\parallel[x_\alpha,y_\alpha;s]}{k_BT}=\int_0^s\frac{3}{2a^2N}[|x'_\alpha(t)|^2+|y'_\alpha(t)|^2]dt, \tag{1}$$

depending only on $x_\alpha(t)$ and $y_\alpha(t)$, and a perpendicular contribution,

$$\frac{\hat{E}_\perp[z_\alpha;s]}{k_BT}=\int_0^s\left[\frac{3}{2a^2N}|z'_\alpha(t)|^2+w(z_\alpha(t))\right]dt, \tag{2}$$

involving only $z_\alpha(t)$. Thus, the partition function for this chain fragment can written as

$$q(z,z_0,s)\propto\int\mathcal{D}\mathbf{r}_\alpha\exp\left\{-\frac{\hat{E}_\parallel[x_\alpha,y_\alpha;s]+\hat{E}_\perp[z_\alpha;s]}{k_BT}\right\}\times\delta(z_\alpha(0)-z_0)\delta(z_\alpha(s)-z), \tag{3}$$

$$\propto\int\mathcal{D}z_\alpha\exp\left\{-\frac{\hat{E}_\perp[z_\alpha;s]}{k_BT}\right\}\times\delta(z_\alpha(0)-z_0)\delta(z_\alpha(s)-z), \tag{4}$$

where the simplification results due to the fact that the functional integrals over $x_\alpha(t)$ and $y_\alpha(t)$ yield irrelevant constants. The remaining functional integral is then evaluated by the standard method[4,11] of solving a modified diffusion equation,

$$\frac{\partial}{\partial s}q(z,z_0,s)=\frac{a^2N}{6}\frac{\partial^2}{\partial z^2}q(z,z_0,s)-w(z)q(z,z_0,s), \tag{5}$$

with periodic boundary conditions at $z=0$ and $z=2L$ and an initial condition $q(z,z_0,0)=\delta(z-z_0)aN^{1/2}$.

With $q(z,z_0,s)$ in hand, we are now prepared to consider a complete chain of N segments extending from $z=z_0$ to the substrate at $z=0$. In order to specify a particular segment, we parametrize the chain with a variable s that increases from 0 to 1 as the chain is traversed from its $z=z_0$ end towards its $z=0$ end. With that, the distribution of the sNth segment can be expressed as

$$\rho(z;z_0,s)=\frac{q(z,z_0,s)q(0,z,1-s)}{q(0,z_0,1)}. \tag{6}$$

It is now a simple matter of integrating to obtain the segment distribution,

$$\phi(z;z_0)=\int_0^1\rho(z;z_0,s)ds, \tag{7}$$

for a single chain extending to $z=z_0$. Furthermore, the free energy of such a chain is given by

$$\frac{f_0(z_0)}{k_BT}=-\ln q(0,z_0,1). \tag{8}$$

Eventually, we will need to decompose this free energy into $f_0(z_0)=f_{0,e}(z_0)+f_{0,w}(z_0)$, where $f_{0,e}(z_0)$ is the *elastic stretching* energy associated with the configurational entropy of the chain, and

$$\frac{f_{0,w}(z_0)}{k_BT}\equiv\frac{1}{aN^{1/2}}\int_0^{2L}w(z)\phi(z,z_0)dz \tag{9}$$

is the contribution attributed to the field.

The next step is to consider a complete brush grafted to the $z=0$ substrate. Naturally, the distribution of its chain ends will obey the Boltzmann weight,

$$g(z_0)=\frac{aN^{1/2}}{\mathcal{Q}}\exp\left[-\frac{f_0(z_0)}{k_BT}\right], \tag{10}$$

where

$$\mathcal{Q}=\int_0^{2L}\exp\left[-\frac{f_0(z_0)}{k_BT}\right]dz_0 \tag{11}$$

is the partition function for a single grafted chain with its $s=0$ end free to sample the entire volume between $z=0$ and $2L$. Given the end-segment distribution, we can then calculate the segment profile,

$$\phi(z)=\frac{L}{a^2N}\int_0^{2L} g(z_0)\phi(z;z_0)dz_0, \tag{12}$$

of the entire brush.

Of course, the brush attached to the substrate at $z=2L$ is identical to the one at $z=0$. Given this and the fact that polymer melts are effectively incompressible, we require

$$\phi(z)+\phi(2L-z)=1, \tag{13}$$

which provides the self-consistent condition used to evaluate $w(z)$. Once $w(z)$ has been self-consistently determined, the free energy per chain is given by $f=f_e+f_g$, where

$$f_e=\frac{1}{aN^{1/2}}\int_0^{2L} g(z_0)f_{0,e}(z_0)dz_0 \tag{14}$$

is the average elastic energy and

$$f_g=\frac{k_BT}{aN^{1/2}}\int_0^{2L} g(z_0)\ln g(z_0)dz_0 \tag{15}$$

is the entropic contribution due to the free ends.

Our actual implementation of SCFT follows the Fourier approach described in Ref. 4. This, in fact, involves one small modification to the above theory, in that we attach the chains to the substrates with a stiff harmonic potential rather than by a Dirac delta function. This implementation is slightly more involved in that it requires a second partial partition function, $q^\dagger(z,s)$, satisfying the same diffusion, Eq. (5), but with an initial condition, $q^\dagger(z,0)\propto\exp(-\Lambda z^2/a^2)$. By doing this, we avoid undesirable infinities in $w(z)$ that would otherwise occur at $z=0$ and $z=2L$.[8] Nevertheless, because we select an extremely large *spring* constant, $\Lambda N=10^4$, none of the other relevant quantities are noticeably affected.

III. STRONG-STRETCHING THEORY

We now derive the strong-stretching theory (SST) for the same brush system considered in the preceding section. Rather than following the derivation in Ref. 6 based on the original approach by Semenov,[2] a simpler derivation is presented based on the alternate approach introduced by Milner *et al.*[12] This begins by realizing that, in the strong-stretching limit, the partition function, $q(0,z_0,1)$, is dominated by the path, $z_\alpha(s)$, that minimizes $\hat{E}_\perp[z_\alpha;1]$ defined in Eq. (2). As a consequence, the energy of this single path provides an accurate approximation for $f_0(z_0)$. Furthermore, by good fortune, this particular path is easily obtained by making a simple analogy with classical mechanics. If we interpret s as time and $z_\alpha(s)$ as the position of a particle with mass $3/Na^2$, then Eq. (2) corresponds to the action of the particle in a potential $-w(z)$.[13] Hence, the problem of determining the polymer path of lowest energy is equivalent to a standard classical mechanics problem of a particle sliding down a hill (see Fig. 1).

By applying conservation of energy to our imaginary particle, it immediately follows that

$$\frac{3}{2}\left(\frac{z'}{aN^{1/2}}\right)^2-w(z)=\frac{3}{2}v^2(z_0)-w(z_0), \tag{16}$$

where $v(z_0)\equiv(z'|_{z=z_0})/aN^{1/2}$ is a dimensionless initial velocity. We choose a sign convention such that $v(z_0)<0$ if the particle starts off moving away from the substrate, and $v(z_0)>0$ for a velocity towards the substrate. According to Eq. (16), the dimensionless speed as a function of position z is given by

$$S(z;z_0)\equiv\frac{|z'|}{aN^{1/2}}=\left(v^2(z_0)-\frac{2}{3}[w(z_0)-w(z)]\right)^{1/2}. \tag{17}$$

In the event that the particle begins with a negative velocity, the trajectory first extends outward to $z=z_m$ as determined by $S(z_m;z_0)=0$, before it reverses direction towards the substrate. Otherwise, the maximum extent of the trajectory is simply $z_m=z_0$.

The concentration of segments along the polymer path is given by $N|ds/dz|$, which is inversely proportional to the speed of our imaginary particle. Thus, the segment distribution for a chain starting from z_0 is given by

$$\phi(z;z_0)=\begin{cases}1/S(z;z_0), & \text{if } 0<z<z_0,\\ 2/S(z;z_0), & \text{if } z_0<z<z_m,\\ 0, & \text{if } z_m<z.\end{cases} \tag{18}$$

The factor of 2 for the case, $z_0<z<z_m$, follows from the fact that the trajectory transverses the interval in both directions. By noting that the total number of segments in a chain is N, we obtain the constraint,

$$\frac{1}{aN^{1/2}}\int_0^{2L}\phi(z;z_0)dz=1, \tag{19}$$

which is used to determine the initial velocity, $v(z_0)$.

For any given z_0, we can now calculate the lowest-energy path $z_\alpha(s)$, generally referred to as the *classical* trajectory. With that, it is a straightforward matter to calculate its corresponding energy, $f_0(z_0)\equiv f_{0,e}(z_0)+f_{0,w}(z_0)$. The elastic contribution is given by

$$\frac{f_{0,e}(z_0)}{k_BT}\equiv\frac{3}{2a^2N}\int_0^1|z'_\alpha(s)|^2\,ds=\frac{3}{2aN^{1/2}}\int_0^{2L}\frac{dz}{\phi(z;z_0)}, \tag{20}$$

and the field energy, $f_{0,w}(z_0)$, is again given by Eq. (9). From here on, SST proceeds in the exact same way as SCFT.

IV. RESULTS

To begin, we evaluate the field, $w(z)$, self-consistently by requiring the two brushes to fill space uniformly such that Eq. (13) is satisfied. The solid curves in Fig. 2 show the resulting SST field for two different brush thicknesses, L. Note that the axes have been scaled so as to stress the convergence towards the $L\to\infty$ limit,

$$w(z)\to\begin{cases}-\dfrac{3\pi^2z^2}{8a^2N}, & \text{if } 0<z<L,\\ -\dfrac{3\pi^2(2L-z)^2}{8a^2N}, & \text{if } L<z<2L,\end{cases} \tag{21}$$

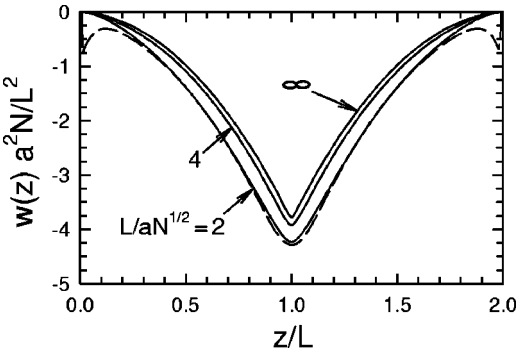

FIG. 2. Self-consistent field, $w(z)$, plotted between the two substrates at $z=0$ and $z=2L$. The solid curves show the SST field for a series of brush thicknesses, while the dashed curve shows the SCFT result for $L/aN^{1/2}=2$. The $L\to\infty$ limit of SST is obtained from Eq. (21).

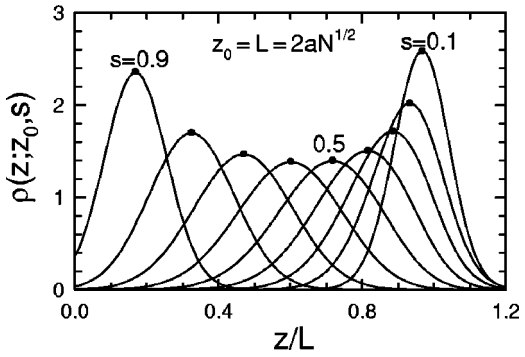

FIG. 4. Distribution of the sN'th segment for $s=0.1, 0.2, \ldots, 0.9$, calculated with SCFT for a chain stretched to $z_0/aN^{1/2}=2$ within a brush of thickness $L/aN^{1/2}=2$. The SCFT trajectory, $z_\alpha(s)$, is defined by the peak positions denoted by solid dots.

which is the well known result that occurs when the end-segment entropy is ignored.[14] Unfortunately, numerical limitations prevent us from solving the SCFT to the same degrees of stretching, but nevertheless we are able to evaluate the field for $L/aN^{1/2}=2$; the result is displayed in Fig. 2 with a dashed curve. The SCFT prediction compares well with that of SST, except at the two grafting surfaces; this discrepancy will be explained in the following section.

The entropy of the free ends creates an effective force acting on the tip of each chain. In SST, this entropic force is proportional to the initial velocity, $v(z_0)$, of our imaginary particle, which is displayed in Fig. 3 as a function of the end position, z_0, for two different brush thicknesses. Again, the axes are scaled so as to illustrate convergence to the $L\to\infty$ limit,

$$v(z_0)\to\begin{cases} 0, & \text{if } 0<z<L, \\ \dfrac{\pi\sqrt{p^2-z_0^2}}{2aN^{1/2}}, & \text{if } L<z<2L, \end{cases} \tag{22}$$

where p satisfies

$$2\sin^{-1}\left(\frac{L}{p}\right)-\sin^{-1}\left(\frac{2L-z_0}{p}\right)=\frac{\pi}{2}, \tag{23}$$

which is well approximated by

$$p\approx L+\frac{1}{3}(z_0-L)+\frac{2}{27L}(z_0-L)^2. \tag{24}$$

Based on Fig. 3, the weakly stretched chains have a negative entropic force at their end causing a nonmonotonic trajectory, while the more strongly stretched chains have a positive force resulting in a monotonic trajectory. It will turn out that the division between these two cases coincides with the peak in the end-segment distribution function, $g(z_0)$.[15]

In SST, inverting the polymer trajectory, $z_\alpha(s)$, identifies a specific position for each segment in the chain. On the other hand, in SCFT, the sN'th segment occupies a distribution of positions as illustrated in Fig. 4 for the case $z_0=L=2aN^{1/2}$. These distributions are approximately Gaussian[16] with a well-defined peak corresponding to the most likely position. Based on the maximum, we can define a SCFT trajectory, $z_\alpha(s)$, to compare with the SST prediction. As demonstrated in Fig. 5, the agreement is remarkably good, particularly in regards to the nonmonotonic trajectories at small z_0 where $z_m>z_0$. For a chain with $z_0/aN^{1/2}=0.5$, SCFT predicts the point of maximum extent to occur at $s=0.129$ and $z_m/aN^{1/2}=0.513$, which compares well with the SST prediction of $s=0.140$ and $z_m/aN^{1/2}=0.516$. Inter-

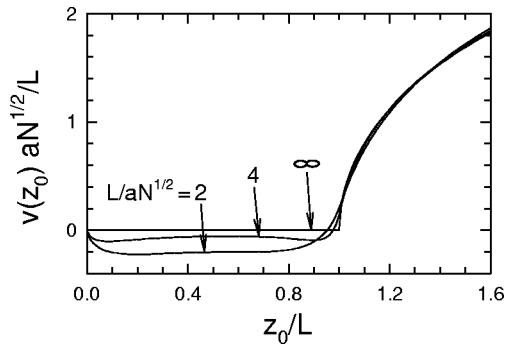

FIG. 3. Entropic force, $v(z_0)$, at the free end of a chain as a function of its position, z_0, calculated with SST. The $L\to\infty$ limit is obtained from Eqs. (22) and (23).

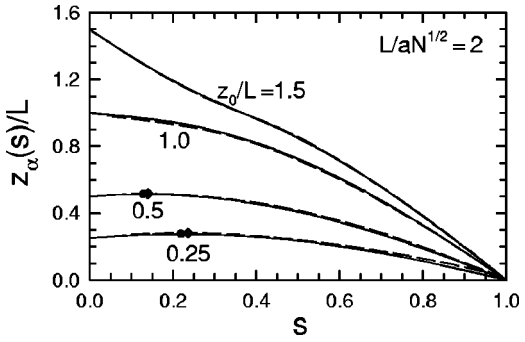

FIG. 5. Polymer trajectories, $z_\alpha(s)$, for various end positions, z_0, within a brush of thickness $L/aN^{1/2}=2$. The solid and dashed curves are obtained from SST and SCFT, respectively. For the less stretched chains, where the trajectory starts off by moving away from the substrate, the circles and diamonds denote the points at which the trajectory reverses direction as calculated by SST and SCFT, respectively.

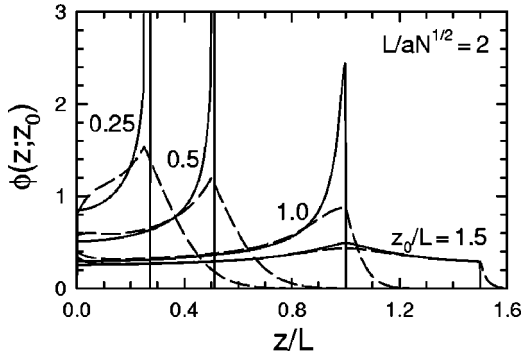

FIG. 6. Segment profiles, $\phi(z;z_0)$, for chains with various end positions, z_0, within a brush of thickness $L/aN^{1/2}=2$. The solid and dashed curves are obtained from SST and SCFT, respectively.

estingly, even though a significant duration of the trajectory can elapse before reaching the turning point, z_m does not generally exceed z_0 by very much.

Figure 6 examines the segment distribution, $\phi(z;z_0)$, of an entire chain as a function of its end position, z_0. Not too surprisingly, SCFT and SST produce consistent results for the highly stretched chains such as $z_0/L=1.5$. However, the results differ substantially for those chains with a nonmonotonic trajectory. In this case, SST predicts an infinite spike in $\phi(z;z_0)$ at $z=z_m$, whereas SCFT does not. This inconsistency will ultimately result in an inaccurate SST prediction for the overall brush profile, $\phi(z)$.

The elastic and field contributions to the free energy are plotted as a function of the end position, z_0, in Figs. 7(a) and 7(b), respectively. The solid curves show the SST results for

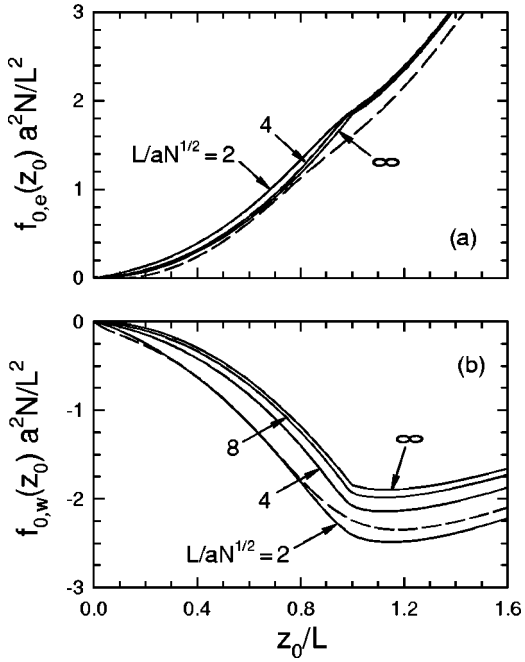

FIG. 7. (a) Elastic energy, $f_{0,e}(z_0)$, of a chain as a function of its extension, z_0, plotted for a series of brush thicknesses using SST (solid curves) and for $L/aN^{1/2}=2$ using SCFT (dashed curve). The $L\to\infty$ limit of SST is given by Eq. (25). (b) Analogous plot for the field energy, $f_{0,w}(z_0)$. In this case, the $L\to\infty$ limit is given by Eq. (26).

a selection of brush thicknesses. As before, the axes are scaled so as highlight the convergence to the $L\to\infty$ limits given by

$$\frac{f_{0,e}(z_0)}{k_BT}\to\begin{cases}\dfrac{3\pi^2 z_0^2}{16a^2N}, & \text{if } 0<z<L,\\ \dfrac{3\pi}{16a^2N}(\pi p^2+P^2), & \text{if } L<z<2L,\end{cases} \tag{25}$$

and

$$\frac{f_{0,w}(z_0)}{k_BT}\to\begin{cases}-\dfrac{3\pi^2 z_0^2}{16a^2N}, & \text{if } 0<z<L,\\ -\dfrac{3\pi}{16a^2N}(\pi p^2-P^2), & \text{if } L<z<2L,\end{cases} \tag{26}$$

where

$$P^2=4L\sqrt{p^2-L^2}+2(2L-z_0)\sqrt{p^2-(2L-z_0)^2}, \tag{27}$$

$$\approx\frac{16}{3}\left(\frac{2}{3}\right)^{1/2}(z_0-L)^{3/2}L^{1/2}. \tag{28}$$

For the thinner $L/aN^{1/2}=2$ brush, we plot the SCFT predictions with dashed curves. In this case, the agreement with SST is reasonable, but not particularly impressive.

Given the free energy, $f_0(z_0)\equiv f_{0,e}(z_0)+f_{0,w}(z_0)$, of extending a chain end to $z=z_0$, the end-segment distribution function, $g(z_0)$, is obtained immediately from Eq. (10). The SST prediction is plotted in Fig. 8(a) with solid curves for a series of brush thicknesses, L. In the $L\to\infty$ limit, the distribution approaches the well-known result,

$$g(z_0)\to\begin{cases}\dfrac{z_0aN^{1/2}}{L\sqrt{L^2-z_0^2}}, & \text{if } 0<z<L,\\ 0, & \text{if } L<z<2L,\end{cases} \tag{29}$$

obtained when the entropy of the chain ends is ignored.[14] Clearly, the inclusion of chain-end entropy produces a dramatic effect on $g(z_0)$, particularly for the thinner brush with $L/aN^{1/2}=2$. Without it, the SST distribution in Eq. (29) would bare no resemblance to the SCFT prediction denoted by the dashed curve, whereas with the correction, the agreement is quite good.

As we have just seen, the chain-end entropy causes $g(z_0)$ to extend beyond the midplane producing an exponentially decaying tail. By using Eqs. (25) and (26) for the large L behavior of $f_{0,e}$ and $f_{0,w}$, it follows that

$$g(z_0)\approx g(L)\exp\left[-\frac{3\pi P^2}{8a^2N}\right]$$

$$\approx g(L)\exp[-5.13(z_0-L)^{3/2}L^{1/2}/a^2N], \tag{30}$$

for $z_0>L$. Based on this functional form, the tails of $g(z_0)$ should collapse onto a single master curve when plotted as a function of $(z_0-L)L^{1/3}$, and indeed this is confirmed by Fig. 8(b). From that, it follows that the penetration depth of the $g(z_0)$ distribution beyond the midplane scales as $L^{-1/3}$.

Our expression in Eq. (30) still contains the unknown prefactor, $g(L)$, which has to be determined by the normal-

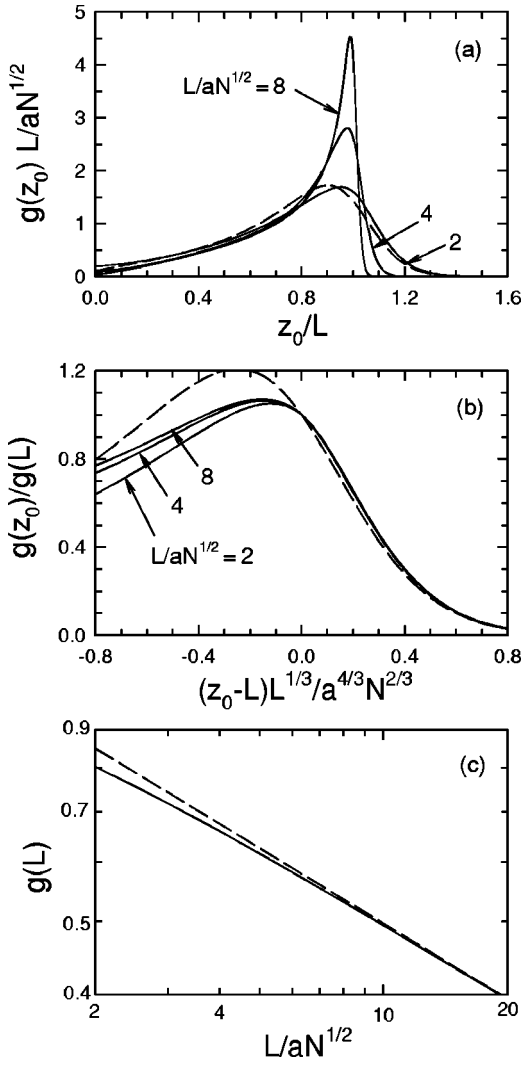

FIG. 8. (a) End-segment distribution function, $g(z_0)$, plotted for several brush thicknesses using SST (solid curves) and for $L/aN^{1/2}=2$ using SCFT (dashed curve). (b) The same results plotted in terms of a scaling variable. (c) Logarithmic plot of the end-segment distribution function at the midplane. The dashed line corresponds to the fit, $g(L)\approx 1.07(L/aN^{1/2})^{-1/3}$.

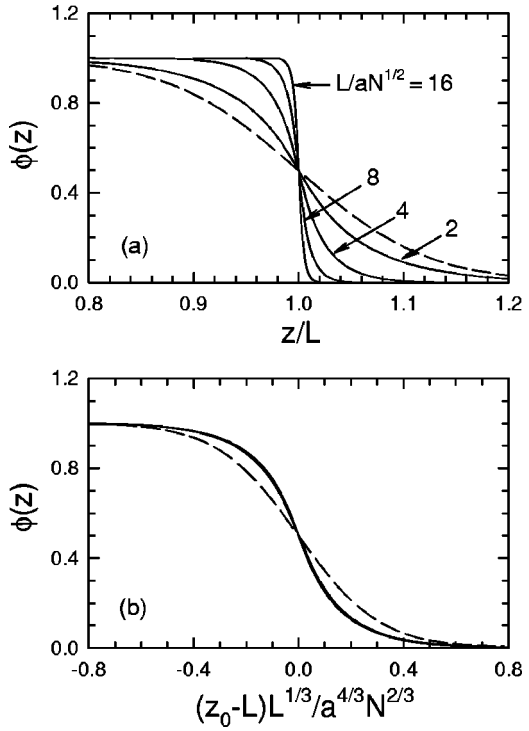

FIG. 9. (a) Brush profile, $\phi(z)$, plotted for several brush thicknesses using SST (solid curves) and for $L/aN^{1/2}=2$ using SCFT (dashed curve). (b) The same results plotted in terms of a scaling variable.

ization condition, $\int g(z_0)dz_0=aN^{1/2}$. However, for that, we need an expression for $g(z_0)$ over the entire range $0<z_0<2L$. If we make the sensible assumption that the main effect of finite L is to truncate the peak in $g(z_0)$ in order to create the tail, we can then approximate $g(z_0)$ by Eq. (29) for $0<z_0<(1-\epsilon)L$, by $g(L)$ for $(1-\epsilon)L<z_0<L$, and by Eq. (30) for $L<z_0$. If we also require $g(z_0)$ be continuous, it follows that $g(L)\propto L^{-1/3}$. Indeed, the logarithmic plot in Fig. 8(c) confirms this scaling and extracts a numerical value for the proportionality constant.

With the end-segment distribution in hand, the brush profile is calculated by performing the simple integration in Eq. (12). The result is displayed in Fig. 9(a) for a series of L, and as expected, the profile approaches a step function in the $L\to\infty$ limit. Based on the functional dependence of $g(z_0)$, the brush profiles should also collapse onto a single master curve when plotted as a function of $(z_0-L)L^{1/3}$, as confirmed by Fig. 9(b). Hence, the penetration depth of $\phi(z)$ will also scale as $L^{-1/3}$ as it did for $g(z_0)$. However, this time we do not obtain a simple functional approximation for the master curve.

The dashed curves in Fig. 9 show the more accurate profile, $\phi(z)$, as calculated by SCFT for $L/aN^{1/2}=2$. Although the agreement is not terrible, SST still significantly underestimates the degree of interpenetration between the two brushes. This can be attributed to the inaccurate SST predictions for the single chain profiles, $\phi(z;z_0)$, plotted in Fig. 6.

We are finally at the point where the free energy of the entire polymer brush can be calculated. The average energy per chain, $f=f_e+f_g$, is conveniently expressed as

$$\frac{f}{k_BT}=\frac{\pi^2L^2}{8a^2N}-\ln\left(\frac{L}{2aN^{1/2}}\right)+\frac{\Delta f}{k_BT}, \tag{31}$$

where the first and second terms are the $L\to\infty$ limits of f_e and f_g, respectively, obtained by inserting Eqs. (25) and (29) into Eqs. (14) and (15). The residual term, Δf, is identified as the free-energy correction for finite L, which according to Likhtman and Semenov,[8] should scale as $L^{-2/3}$ at large L. This is confirmed by the logarithmic plot in Fig. 10, where the large L regime is well approximated by the dashed line corresponding to $\Delta f/k_BT\approx -0.84(L/aN^{1/2})^{-2/3}$. This residual is significantly larger than the previous estimate, $\Delta f/k_BT\approx -0.37(L/aN^{1/2})^{-2/3}$, in Ref. 8, where the effect on $w(z)$ was not taken into account.[16] Nevertheless, our finite-stretching correction to the free energy still omits two important contributions, which we discuss in the following section.

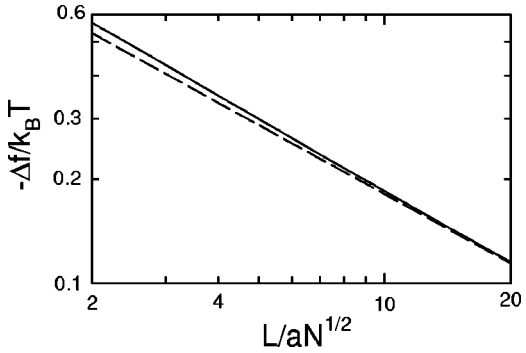

FIG. 10. Logarithmic plot of the SST free-energy correction, Δf, associated with the end-segment entropy as a function of the brush thickness, L. The dashed line corresponds to the fit, $\Delta f/k_BT \approx -0.84(L/aN^{1/2})^{-2/3}$.

V. DISCUSSION

The scaling relations involving the end-segment distribution function, $g(z_0)$, the brush profile, $\phi(z)$, and the free energy per chain, f, have been previously anticipated.[8,9] However, we are now able to provide accurate values for the proportionality constants due to the fact we have performed a full numerical treatment of the end-segment entropy. As a result, we find that the magnitude of the free-energy correction, Δf, is more than twice[17] that estimated in Ref. 8. Nevertheless, our most significant prediction is that the scaling relations remain accurate down to experimentally realistic brush thicknesses, i.e., $L \lesssim aN^{1/2}$. In reality, we should not have expected the master curves for $g(z_0)$ in Figs. 8(b) and $\phi(z)$ in Fig. 9(b) to be accurate for such narrow brushes as $L=2aN^{1/2}$. Likewise, it is impressive that the power-law behaviors for $g(L)$ in Fig. 8(c) and Δf in Fig. 10 remain accurate to $\sim 10\%$ even at $L=2aN^{1/2}$. This is indeed extremely fortunate for SST. Had these scaling relations failed to be accurate thus requiring SST to be implemented numerically for experimentally relevant conditions, then there would be no real justification for using SST rather than the full SCFT.

With the end-segment entropy taken care of, it only remains to consider fluctuations about the classical (i.e., most probable) trajectories. As pointed out previously,[7,14,16] their inclusion transforms SST into SCFT in the same way that classical mechanics transforms into quantum mechanics. Thus, we can potentially invoke the mathematical machinery, such as perturbation theory and the WKB approximation, already developed for quantum mechanics.[7] For instance, Milner[16] has been able to predict accurate distributions for $\rho(z;z_0,s)$ based on the known quantum-mechanical solution for a parabolic potential. Correcting the delta-function distribution for $\rho(z;z_0,s)$ will clearly resolve much of the remaining discrepancy in Fig. 6 between the SST and SCFT predictions for $\phi(z;z_0)$. This should broaden the SST prediction for the brush profile, $\phi(z)$, in Fig. 9, which in turn will modify the SST potential, $w(z)$, near the midplane, presumably bringing it into better agreement with SCFT. Furthermore, Goveas and Milner[7] predict that this will also provide an additional free-energy contribution slightly dominating the one considered here in Fig. 10.

As pointed out earlier, there is also a sizable discrepancy between SST and SCFT in regards to $w(z)$ near the two substrates (see Fig. 2). While SST predicts a smooth monotonic potential, the SCFT potential shows a dip as each substrate is approached followed by a large positive delta-like contribution at the substrate. In Fig. 2, the base of the delta-like contribution can be seen due to its small but finite width. Had we attached the chains to the substrate rigidly rather than with stiff springs (see the last paragraph in Sec. II), the field would contain a true delta function at each substrate. As it turns out, this behavior has already been anticipated by Likhtman and Semenov.[8] It results due to the fact that fluctuations about the classical trajectories tend to increase the number of segments deposited next to the substrates. This has to be countered by adding delta functions to the potential along with a negative finite contribution that extends over regions, $0<z\lesssim\mu$ and $2L-\mu\lesssim z<2L$, referred to as *proximal* layers. The width of the two proximal layers is expected to scale as $\mu \propto L^{-1}$, and furthermore their effect presumably provides the dominant free-energy correction to SST. Certainly, the predictions in Ref. 8 are qualitatively consistent with our SCFT results, but it still remains to test them quantitatively. That we save that for a future publication.

VI. CONCLUSIONS

This paper has examined the corrections to strong-stretching theory (SST) resulting from end-segment entropy in the context of two opposing brushes each of thickness, L. The effectiveness of these corrections was assessed by direct comparisons with full mean-field calculations using self-consistent field theory (SCFT). The most notable improvement involves the end-segment distribution function, $g(z_0)$, as demonstrated earlier in Ref. 6. Furthermore, we find that it produces a sizable deviation from the conventional parabolic potential, Eq. (21), in good agreement with SCFT. Another interesting consequence is the introduction of nonmonotonic trajectories[10] (see Fig. 5), once again in agreement with SCFT.

The present study reconfirms several previous scaling predictions. In particular, the penetration depth beyond the midplane of the end-segment distribution function, $g(x)$, and the brush profile, $\phi(z)$, both scale as $L^{-1/3}$.[8,9] We also show that the concentration of end segments at the midplane, $g(L)$, scales as $L^{-1/3}$. As anticipated by Likhtman and Semenov,[8] the free-energy correction per chain is found to involve a trivial logarithm contribution plus a power-law contribution that scales as $L^{-2/3}$. Because we have performed a full numerical treatment, we could also accurately predict the proportionality factors. More importantly, our study demonstrates that these scaling relations remain accurate down to experimentally relevant grafting densities, i.e., $L/aN^{1/2} \lesssim 1$.

Although the present corrections have dramatically improved the agreement between SST and SCFT, there are at least two other important effects that need to be considered partly because of their more dominant free-energy contributions.[7,8] In addition to their effect on the free energy, fluctuations about the about the most probable paths[7,16] should increase the penetration depth of $\phi(z)$ towards the

SCFT prediction and presumably improve $w(z)$ in the vicinity of the midplane. The more important consideration is likely the proximal layer near each substrate, where $w(z)$ has to be significantly modified in order to prevent the fluctuations from causing an over accumulation of segments.[8] Although it remains to be seen, these corrections could lead to a very powerful version of SST capable of providing accurate analytical predictions applicable to experimentally relevant conditions.

ACKNOWLEDGMENTS

We are grateful for valuable discussions with Sasha Semenov regarding the proximal layers. This work was supported by the EPSRC (GR/M61160)

[1] S. F. Edwards, Proc. Phys. Soc. London **85**, 613 (1965).
[2] A. N. Semenov, Sov. Phys. JETP **61**, 733 (1985).
[3] M. W. Matsen, J. Phys.: Condens. Matter **14**, R21 (2002).
[4] M. W. Matsen and J. M. Gardiner, J. Chem. Phys. **115**, 2794 (2001).
[5] M. W. Matsen and M. D. Whitmore, J. Chem. Phys. **105**, 9698 (1996); M. W. Matsen, *ibid.* **114**, 10528 (2001).
[6] M. W. Matsen and F. S. Bates, Macromolecules **28**, 8884 (1995).
[7] J. L. Goveas, S. T. Milner, and W. B. Russel, Macromolecules **30**, 5541 (1997).
[8] A. E. Likhtman and A. N. Semenov, Europhys. Lett. **51**, 307 (2000).
[9] T. A. Witten, L. Leibler, and P. A. Pincus, Macromolecules **23**, 824 (1990).
[10] R. R. Netz and M. Schick, Europhys. Lett. **38**, 37 (1997); Macromolecules **31**, 5105 (1998).
[11] E. Helfand, J. Chem. Phys. **62**, 999 (1975).
[12] S. T. Milner, T. A. Witten, and M. E. Cates, Macromolecules **21**, 2610 (1988).
[13] H. Goldstein, *Classical Mechanics*, 2nd ed. (Addison-Wesley, Philippines, 1980).
[14] S. T. Milner, Science **251**, 905 (1991).
[15] A. Johner and J. F. Joanny, J. Chem. Phys. **98**, 1647 (1993).
[16] S. T. Milner, J. Chem. Soc., Faraday Trans. **86**, 1349 (1990).
[17] In order to compare our results with those in Ref. 8, a couple differences must be taken into account. First, our $g(z_0)$ in Eq. (10) is only defined for positive z_0 and includes a factor $aN^{1/2}$ to make it dimensionless. Second, our definition of a differs by a factor of $\sqrt{6}$.